Goulet, J.-A., Texier, M., Michel, C., Smith, I., and Chouinard, L. (2014). Quantifying the effect of modelling simplifications for structural identification of bridges. Journal of Bridge Engineering, 19(1):59–71.

Quantifying the effects of modeling simplifications for structural identification of bridges

James-A. Goulet A. M. ASCE[1], Marie Texier[2], Clotaire Michel[3], Ian F. C. Smith, F. ASCE[4] and Luc Chouinard [5]

Abstract

Several long span prestressed segmental box girder bridges were built in the early 1980's and many of them are affected by long-term residual deformations. Although models have been proposed to describe their structural behavior, several uncertainties remain. This paper examines the effects of errors introduced by model simplifications on predicted values. These results are used to improve the estimation of parameter values using model-based data-interpretation strategies. The procedure is illustrated for the Grand-Mere bridge located in Canada. This bridge is affected by excessive long-term vertical displacements. Model simplifications such as the degree of complexity of a model are found to have an important influence on prediction errors. Representing these errors by zero-mean independent Gaussian noise does not adequately describe the relationships between errors observed in this case study. Estimated errors are used during the interpretation of ambient vibration acceleration data recorded on the structure. The interpretation approach employed is based on error-domain model falsification. The study provides ranges of parameter values that can subsequently be used to characterize more accurately aspects such as long-term creep and shrinkage behavior.

Keywords: Structural identification, model simplification, uncertainties, error-domain model falsification, ambient vibration monitoring, bridge, Finite elements

[1]Former PhD. student, Applied Computing and Mechanics Laboratory, École Polytechnique Fédérale de Lausanne (EPFL), School of Architecture, Civil and Environmental Engineering, Lausanne, Switzerland (corresponding author). E-mail: James.A.Goulet@gmail.com

[2]Former Master student, Applied Computing and Mechanics Laboratory, École Polytechnique Fédérale de Lausanne (EPFL), School of Architecture, Civil and Environmental Engineering, Lausanne, Switzerland

[3]Researcher, Swiss Federal Institute of Technology Zurich (ETHZ), Zurich, Switzerland

[4]Professor, Applied Computing and Mechanics Laboratory, École Polytechnique Fédérale de Lausanne (EPFL), School of Architecture, Civil and Environmental Engineering, Lausanne, Switzerland

[5]Professor, Department of Civil Engineering and Applied Mechanics, McGill University, Montréal, Canada

INTRODUCTION

Challenges associated with the preservation of aging existing structures require a deeper understanding of structural behavior than what is required for design purposes. Model-based structural identification compares model predictions with measurements to infer the properties of structures and phenomena that influence structural behavior.

Many applications of structural identification are described in a recent state-of-the-art review by Catbas et al. (2012). Traditional approaches generally assume that the combination of modeling and measuring uncertainties can be represented by Gaussian noise, independently affecting measurements and predictions. In most cases, the error term does not include the systematic bias in model predictions due to omissions and simplifications. This is because models are assumed to have been validated (Oberkampf and Trucano 2008; Sankararaman and Mahadevan 2011; Mottershead et al. 2011). For civil-engineering structures, it is often difficult to validate models to the point where the only discrepancy between predictions and measurements is due to the choice of parameter values and measurement uncertainty. Little work has been done to quantify uncertainties related to model simplifications. Exceptions include Nowak et al. (1985, 1998, 2004) who studied the importance of some secondary structural elements in bridge models. Results indicated that for the structure studied, secondary elements may have an effect up to 40% on the girder distribution factor. Also, studies on mesh refinement have been performed by Topkaya et al. (2008) who recommended the usage of 9-node shell of size no larger than 1.5 m for the analysis medium span bridges (60-120 m).

This paper includes a study of the influence of modeling simplifications on static and dynamic prediction errors. These results are then used as a starting point to assess the condition of the Grand-Mere Bridge using ambient vibration monitoring. The first section of the paper presents the structural identification methodology. In the second section, the effect of modeling simplifications on predicted values is examined using the Grand-Mere Bridge as a case-study. This involves the comparison of model predictions for several levels of complexity and for combinations of element types. The third section presents the condition assessment of the Grand-Mere Bridge using ambient vibration monitoring data.

ERROR-DOMAIN MODEL FALSIFICATION

The error-domain model falsification approach using ambient vibration monitoring data was developed by Goulet et al. (2012). The concept of error-domain model falsification is based on the generation of possible model instances (sets of parameters represented by the vector $\boldsymbol{\theta}$) using a model class $\mathrm{g}(\boldsymbol{\theta})$; obtain predictions for each of them; and then falsify instances having unacceptable differences (observed residuals) between predictions and measurements. Falsification occurs when an observed residual is outside threshold values that are calculated by combining modeling and measurement uncertainties. The candidate model set is made from all instances that

cannot be falsified. Threshold bounds $T_{low,i}$ and $T_{high,i}$ define to the smallest intervals that simultaneously contain a probability $\phi \in]0,1]$ for the combined uncertainty probability distribution function (*pdf*), $f_{U_{c,i}}(\epsilon_{c,i}), \forall i \in \{1,...,n_m\}$. Here, n_m is the number of comparison points for which predictions and measurements are available. $U_{c,i}$ is a random variable used to represent the possible outcomes of combined error instances $\epsilon_{c,i}$ for comparison point i (the index $_c$ stands either for the combined error or uncertainty).

Threshold bounds having a probability smaller or equal to $1-\phi$ of falsifying a correct model can be defined using the Šidák correction (Šidák 1967). Šidák correction is used in the field of hypothesis testing when multiple comparisons are performed. For practical purposes, threshold bounds can be computed numerically for each comparison point i, as the shortest sets $\{T_{low,i}, T_{high,i}\}$ such as

$$\phi^{1/n_m} = \int_{T_{low,i}}^{T_{high,i}} f_{U_{c,i}}(\epsilon_{c,i}) d\epsilon_{c,i} \; \forall i \in \{1,\ldots,n_m\} \tag{1}$$

A model instance is falsified when Equation 2 is not satisfied; i.e. when the residual between predicted $\mathbf{g}_i(\boldsymbol{\theta})$ and measured y_i values is outside the threshold bounds for any comparison point i.

$$\forall i \in [1,\ldots,n_m] : \; T_{low,i} \leq \mathbf{g}_i(\boldsymbol{\theta}) - y_i \leq T_{high,i} \tag{2}$$

With this methodology, a correct model has a probability smaller or equal to $1-\phi$ to be wrongly falsified. For engineering applications ϕ can be set to 0.95.

In this approach, modeling and measurement errors are combined because during structural identification, residual calculations make them undistinguishable. The probability density functions defining modeling and measurement errors are estimated independently and then combined probabilistically. The combined uncertainty is used to determine the minimal and maximal plausible errors for each comparison point i, i.e. threshold bounds $T_{low,i}$ and $T_{high,i}$. An advantage of this methodology is that it does not require to know the relationships between prediction errors to identify the values of parameters. Multiple prediction locations and predictions types (strains, rotations, frequencies, etc.) are often affected by complex sets of relationships, particularly when models includes significant omissions and simplifications. For full-scale structures the challenge resides in understanding and in quantifying these relationships.

In order to identify parameter values using ambient vibration monitoring as an input, time-domain acceleration data is converted into frequencies and mode shapes. The model falsification process is divided into two steps. First, a correspondence check is performed between the n_y measured mode shapes ($\Phi_{y_j}, j \in \{1,\ldots,n_y\}$) and $n_l \times n_k$ predicted mode shapes ($\Phi_{\mathbf{g}_l(\boldsymbol{\theta_k})}, l \in \{1,\ldots,n_l\}, k \in \{1,\ldots,n_k\}$) to ensure that the right modes are compared. Here, n_l is the number of predicted modes and n_k is the number of model instances. Mode shape comparison is made using the Modal Assurance Criterion (MAC) (Allemang and Brown 1982). The MAC criteria is presented in

Equation 3, where ^{H} denotes complex conjugate transpose.

$$\mathrm{MAC}(\Phi_{y_j}, \Phi_{\mathbf{g}_l(\boldsymbol{\theta}_k)}) = \frac{|\Phi_{y_j}^H \Phi_{\mathbf{g}_l(\boldsymbol{\theta}_k)}|^2}{|\Phi_{y_j}^H \Phi_{y_j}||\Phi_{\mathbf{g}_l(\boldsymbol{\theta}_k)}^H \Phi_{\mathbf{g}_l(\boldsymbol{\theta}_k)}|} \tag{3}$$

Only sets $\{j, k, l\}$ satisfying

$$\{(j,k,l) \in \mathbb{N}^3 : \ \mathrm{MAC}(\Phi_{y_j}, \Phi_{\mathbf{g}_l(\boldsymbol{\theta}_k)}) \geq \phi_{\mathrm{MAC}}\} \tag{4}$$

$\forall j \in \{1, \ldots, n_y\}, k \in \{1, \ldots, n_k\}, l \in \{1, \ldots, n_l\}$ are used to falsify model instances. $\phi_{\mathrm{MAC}} \in]0, 1]$ is a target MAC value used to determine if two mode shapes are similar. Predicted natural frequencies are compared with measurements only for the modes that have passed the MAC test. A complete description of the approach is provided by Goulet et al. (2012).

GRAND-MERE BRIDGE

In this section, the analysis performed on the Grand-Mere bridge is presented. The effects of model simplifications are studied in terms of prediction errors for strain, displacement, rotation and natural frequencies of the structure. Model simplifications are related to the types and configurations of elements used in the models.

Bridge description

The bridge is a three-span prestressed concrete box-girder structure with variable inertia. It was built in 1976-1977 and crosses the St-Maurice river to connect the towns of Grand-Mere (west side) and Saint-Georges (east side). At time of construction, with its main span of 181 m, it was the longest bridge of its type in North America. Figures 1 and 2 present the main dimensions of the structure. Along its length, the structure is symmetric with respect to its stiffness and non-symmetric with respect to its mass due to sand filling in the East-bound direction.

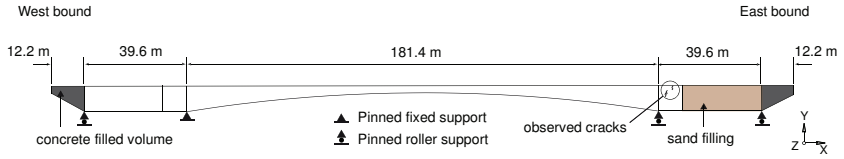

Figure 1. Grand-Mere Bridge elevation view

The bridge experienced problems after completion (Massicotte et al. 1994; Massicotte and Picard 1994). Vertical displacements at mid-span started to increase and in 1987, 10 years after construction, reached 300 mm. Localized cracks appeared on the east side of the bridge (see Figure 1), on the upper deck and on the southern web. In 1992, additional prestressing cables were added, and the cracks, attributed to the

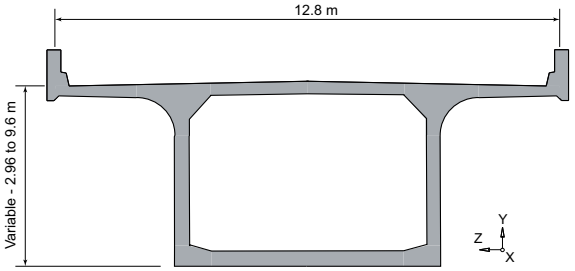

Figure 2. Grand-Mere Bridge cross-section detail

differential shrinkage between the webs and the upper flange of the section, were filled with mortar. The techniques used to strengthen the bridge are described by Massicotte et al. (1994). The causes of these problems were attributed to inaccurate estimates of the loss in prestressing, the use of poor quality materials, and the poor quality control during execution work.

Model-class descriptions

The choice of model-class complexity depends on the goals of the analysis. While it is generally acknowledged that beam-based models are adequate for design purposes, they usually include too many simplifications for structural identification tasks. A more technically specific reason for not using beam-like models for structural identification is because these models do not automatically include the effects of shear lag (Bazant et al. 2008; Bazant et al. 2010). Not including the non-uniform stress distribution caused by shear lag can lead to large prediction biases that would undermine the capacity to identify structural properties. Nevertheless, many other modeling possibilities exist and therefore, the models used in this study are developed to be illustrative examples.

For the Grand-Mere Bridge, three finite-element model classes have been developed based structural drawings: a simplified shell-based model, a composite shell-solid model, and a full solid-based model. In all models, the parabolic shape of the lower flange has been approximated to have a constant radius. Also, sand filling, used as dead weight in the east-bound side-span, is represented in the model using discrete mass elements located on the bottom flange of the girder. The structure has been assumed to be fully prestressed, so pretension forces are not included in the models. Full uncracked sections have been modelled and the prestressing cables were assumed to act elastically. Figure 3 presents a general overview of the finite-element models.

Simplified shell-based model

The shell-based model is built with shell elements as presented in Figure 4(a). This model class is representative of models that are commonly used by researchers and practitioners for the purpose of model calibration and data interpretation. The wedge-

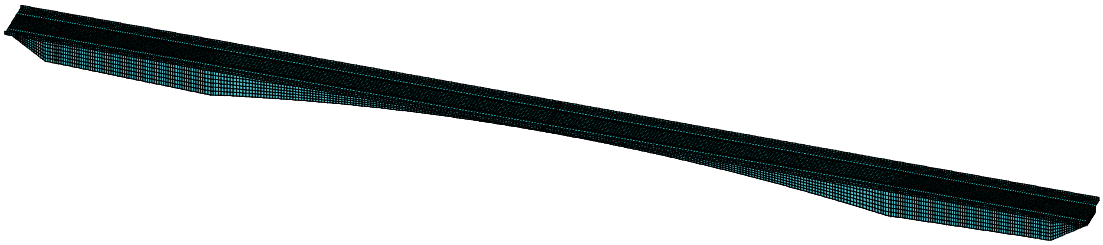

Figure 3. Grand-Mere Bridge finite-element model general overview

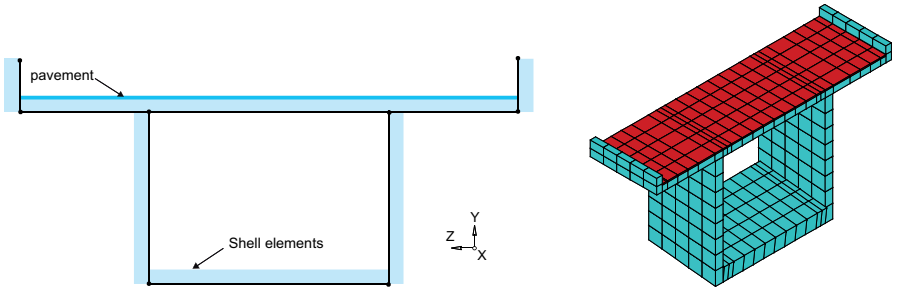

(a) Schematical view of the simplified shell-based model

(b) Cross-section view of the simplified shell-based model

Figure 4. Grand-Mere Bridge cross-section and isometric view of the simplified shell-based model

shaped ends of the structure are made of solid concrete, and are therefore modeled as solid elements. The transversal and longitudinal slopes of the deck are neglected and the openings in the diaphragms are not modeled. The different thicknesses of the cross-sectional elements (web, upper flange and cantilevered deck) are averaged over the length of the bridge. The variation of the lower flange thickness is approximated by stepwise thicknesses changes along the main span. The fillets of the cross-section are not modeled. Support conditions are simplified to linear discrete supports in the transversal direction. The cross-section of the model is presented in Figure 4(b).

Shell-solid model

The shell-solid model is built from a combination of shell and solid elements as presented in Figure 5(a). The level of refinement used in this model class is above what is usually employed in practice because of the increase in modeling and computational effort required. Structural elements that have a small thickness compared to their other dimensions, such as the web, the upper flanges and the cantilevered deck, are modeled as shell elements. Elements having variable thickness are approximated by step-wise constant thicknesses. The wedge-shaped ends are modeled as solid elements, as well as the fillets of the cross-section and the roadway barriers. To ensure the

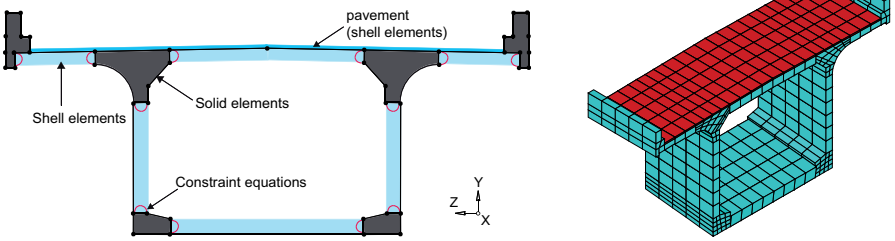

(a) Schematical view of the shell-solid model

(b) Cross-section view of the shell-solid model

Figure 5. Grand-Mere Bridge cross-section and isometric view of the shell-solid model

compatibility between 6 degrees of freedom per node (DOF) shell and 3 DOFs solid elements, constraint equations are applied to the nodes located at the shell-solid interfaces. For support conditions, bearing plates are represented using constraint equations where supports are defined for relevant master nodes only. The cross-section of the shell-solid model is presented in Figure 5(b).

Solid-based model

The solid-based model is built from solid elements as present in Figure 6(a). It is the model with the highest geometrical accuracy. For support conditions, bearing plates are modeled using constraint equations and supports are defined to master nodes only. For the purpose of structural identification, obtaining several thousand solutions from such a complete model class can be computationally prohibitive. The solid-based model cross-section is presented in Figure 6(b). In this model, shell elements are used to represent the pavement layer.

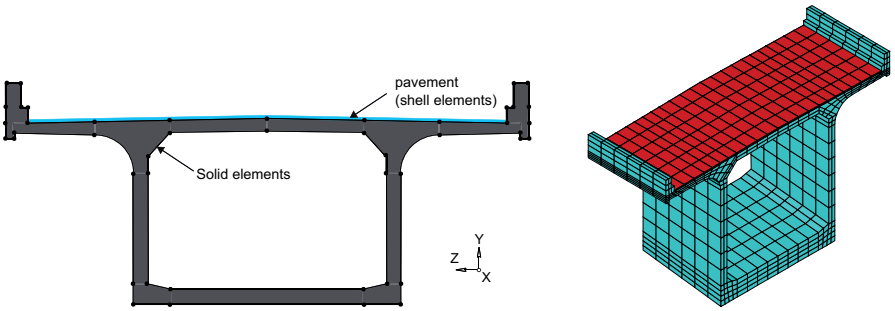

(a) Schematical view of the solid-based model

(b) Cross-section view of the shell-solid model

Figure 6. Grand-Mere Bridge cross-section and isometric view of the solid-based model

Quantification of the effect of model simplifications on prediction errors

In a model, omitting elements and otherwise simplifying the geometry of a structure might modify significantly its mass and stiffness distribution. The effect of model simplifications on both static and dynamic predictions is studied by comparing predicted values from the solid-based model with predictions from less accurate model classes relying on simplifying assumptions. Quantifying errors using the direct comparison of model predictions and measurements may be misleading for two reasons. The first reason is that the correspondence between model predictions and observations only reflects the aggregation of all error sources. In such cases, the validity of the error quantification is limited to the context where measurements were made. The second reason is that all models have inherent uncertainties related to their physical constitutive parameters such as material properties and boundary conditions. Without an accurate knowledge of physical constitutive parameters, it is not possible to quantify the specific contribution of modeling simplifications. The comparison of several model classes is used to estimate the lower bounds associated with model simplification uncertainties and to obtain knowledge of relationships between prediction locations and prediction types. For the comparison of static predictions, loads corresponding to four trucks of 35 Tons each, are positioned at mid-span as presented in Figure 7.

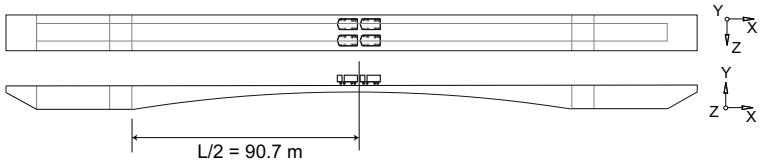

Figure 7. Load-case description for Grand-Mere Bridge

Displacement, rotation and strain predictions obtained from the three model classes described previously are compared in order to observe the effects of model simplifications on the relationships between errors and to obtain a lower-bound estimate for model simplification uncertainties. The results obtained from the simplified shell-based model and the refined shell-based model are compared with those given by the solid-based model according to Equation 5 & 6.

$$\epsilon_{SS,i} = \frac{r_{SS,i} - r_{S,i}}{r_{S,i}} \tag{5}$$

$$\epsilon_{SO,i} = \frac{r_{SO,i} - r_{S,i}}{r_{S,i}} \tag{6}$$

In these equations, $\epsilon_{SS,i}$ $\epsilon_{SO,i}$ are respectively the modeling simplification relative error at location i for shell-solid and shell-based model class. $r_{S,i}$ is the value predicted by the solid model, $r_{SS,i}$ is the value predicted by the shell-solid model and $r_{SO,i}$ is the

value predicted by the shell-based model. The solid model is chosen as a reference because it is the most accurate geometrical representation of the structure.

The most detailed model (i.e. solid-based) is expected to be more rigid than the shell-solid model and the latter more rigid than the shell-based model. This is due to load-carrying elements that are neglected in both the simple shell-solid and shell-based models. More rigid models lead to smaller static predictions and higher natural frequencies. Therefore, modeling simplification errors are expected to be positive for the static predictions, and negative for frequencies. Furthermore, errors are expected to be larger for the shell-based model than with the shell-solid model.

Vertical displacement

Relative errors computed for vertical displacements on the four central prediction locations of the main span are presented in Figure 8. The average relative error on

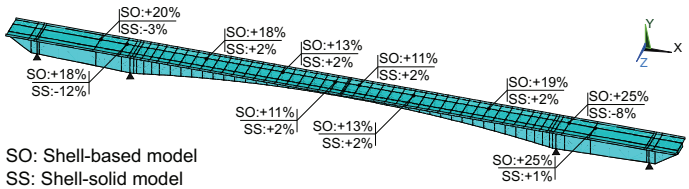

Figure 8. Relative error for vertical displacement predictions due to model simplifications.

the central part of the main span is +12% for the shell-based model, and +2% for the shell-solid model. The error from the shell-based model increases at locations near the intermediate supports. Close to supports the structure has a complex geometry (simultaneous variation in web, lower flange and fillet dimensions) that is not well captured by simplified shell-models.

The errors obtained for the shell-solid model are smaller because less geometrical simplifications are made. In the shell-solid model, negative errors are observed at the supports and on the side spans due model simplifications that affected load redistribution. The relative errors shown in Figure 8 for side-spans are not symmetric due to the lack of symmetry in the load-case. The effect of asymmetry is most visible for side spans because those values are more than 10 times smaller than those predicted in the centre span.

Rotation around Z-axis

Relative errors in rotation predictions around the Z-axis are presented in Figure 9. Errors computed from the shell-based model are all similar with an average value of +10%, except in the zones of intermediate supports where they double. Small variations are obtained in the error given by the shell-solid model. The two values for the central span are of +2%.

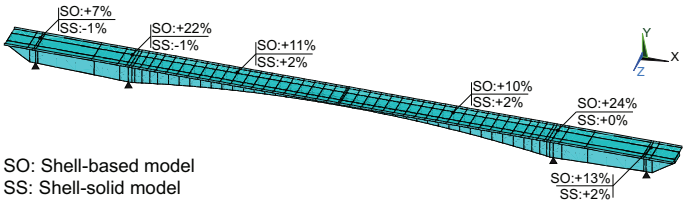

Figure 9. Relative error for rotation predictions around Z-axis due to model simplifications.

Longitudinal strain

Strain relative errors are shown in Figure 10. Predictions for the cantilevered deck are taken on the upper fibre whereas other prediction locations are made on the inside of the box girder. The results obtained show that strain predictions are very sensitive to local model simplifications.

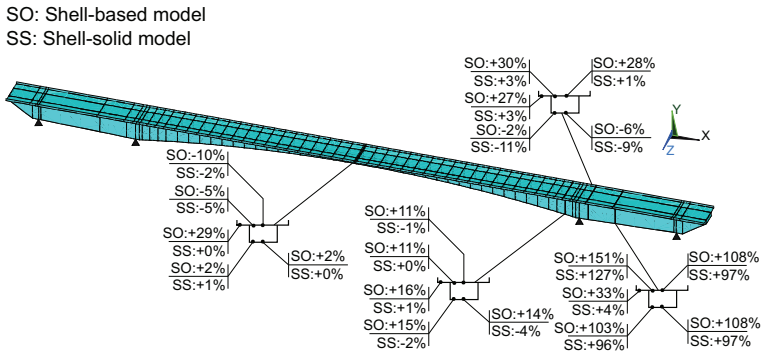

Figure 10. Relative error in strain prediction along X-axis due to model simplifications.

Even if the predicted values are taken at the same locations in the section (e.g. on the upper fibre of the lower deck in the box girder), these locations may not have the same distance to the neutral axis in each model. This is a direct consequence of modeling simplifications. Furthermore, this also affects the load path in the structure. In cases where a single model is calibrated using strain data, such errors may remain unnoticed. Due to the large variability in error values computed, these models may not accurately predict strain patterns in the structure. Therefore, there are non-trivial relationships between errors at several locations and for several predictions types and furthermore errors are not centered on zero.

Dynamic properties

The relative errors for natural frequencies are presented in Table 1. The shell-based

Table 1. Relative error in predicted natural frequencies (%) due to model simplifications and MAC values.

Mode number	Description	Errors in natural frequencies (%)		MAC values	
		Shell-based model	Shell-solid model	Shell-based model	Shell-solid model
1	Vertical bending*	-4.4	-0.5	1.00	1.00
2	Lateral bending*	-4.1	-9.6	1.00	0.99
3	Vertical bending*	-4.4	-1.1	1.00	1.00
4	Lateral bending	-3.1	-16.3	1.00	0.89
5	Vertical bending*	-2.6	-0.2	0.98	0.99
6	Torsion*	-7.5	-18.9	0.99	0.51
	Torsion-2	-	+3.6	-	0.59
7	Vertical bending*	-5.3	-1.4	1.00	1.00
8	Torsion	-8.8	+1.9	0.97	0.61
9	Vertical bending	-6.1	-1.2	0.99	1.00

*: measured mode

model systematically predicts lower frequencies than the solid-based model. In the case of the shell-solid model, prediction errors are smaller than the shell-based model for vertical bending modes. The accuracy of the shell-solid model is less for modes corresponding to lateral bending and torsion.

Mode-shape vectors are extracted for each model and for each natural frequency reported in Table 1. A MAC test is performed on mode shapes. The results of the comparison are shown in Table 1. For the shell-solid model, there are two close modes that present a mix of torsion and lateral bending (Mode 6) and both fail the MAC test with a value below 0.6. Mode number 8 (torsion) also has a poor MAC value. This indicates that torsional behavior is not adequately captured by the refined shell-solid model. Therefore, this model class should not be used to explain observations involving torsional behavior.

A comparison of the mass of the three models reveals that the simplified shell model has a total mass that is 1% lower than the solid model. For the shell-solid model the total mass is 4% lower than the solid model. The solid model has the most accurate mass because it is the most accurate geometric representation of the structure. The simplified shell model has a total mass higher than the shell-solid model because of the approximations made in its transverse and longitudinal cross-sections. For the shell and shell-solid models, the effect of the neglected stiffness partially compensates for the effect of the reduced mass. The relative errors reported in Table 1 include the effects of reduced mass and stiffness.

Result summary

The level of complexity of the model in terms of geometry simplification and element-type combination has a significant influence on predictions. Zones having localized simplifications, such as intermediate supports that present complex geometries, are more sensitive to simplifications and result in higher prediction errors. Fur-

thermore, simplified models may not adequately represent local behavior such as strain for the direct comparison of model predictions with measurements. Prediction errors associated with longitudinal strain may be important ($>$100%) due to local changes in stress distribution that are caused by model simplifications. Global behavior, such as natural frequencies, displacements and rotations around the transversal axis, should be favored as quantities to be compared with measurements during structural identification. Although the solid-based model accurately represents the geometry of the bridge, it remains an approximation of the real structure. Additional errors should be expected between the predictions given by this model and the real behavior. The results of this study provide lower bounds of model simplification errors that can be used for structural identification.

The most important aspect of this study is that it shows that model simplifications and omissions systematically affect the relationships between errors. This means that when an aspect of a structure is neglected in the model, it may systematically affect the prediction errors for several prediction locations and several prediction types to varying degrees. Modeling each of these errors by zero-mean independent Gaussian noise would not represent the relationships between errors observed in this case study.

Structural identification using dynamic data

This section presents the condition evaluation of the Grand-Mere Bridge using ambient vibration monitoring data. A flowchart summarizing the main steps involved in the diagnosis are presented in Figure 11. The first step is to define what parameters need to be identified. These parameters are used to generate a population of model instances that are potentially representative of the structure behavior. Independently, uncertainties involved in the diagnosis are quantified. Modeling uncertainties, such as those arising from the model simplifications estimated in the previous section, are included in the analysis along with measurement uncertainties. All uncertainty sources are combined together and threshold bounds are computed. These thresholds are used when comparing model predictions and measurements to decide which models remain candidates and which are falsified.

Ambient vibration recordings

Ambient vibrations were recorded on the bridge under traffic in 2003. Twelve components were recorded simultaneously during 10 min at a 200 Hz sampling frequency. Seven recording positions with two reference points allowed measurement of 16 points in both vertical and transverse directions plus 28 points in the vertical direction (Figure 12). Accelerometers were positioned inside the box girder on the web faces at about 500 mm above the lower flange.

In order to be interpreted, measured accelerations have to be synthesized into natural frequencies and mode shapes (experimental modal analysis). The technique used here is the Frequency Domain Decomposition (FDD) method (Brincker et al. 2001). This technique was already successfully used for civil structures (Michel et al. 2008;

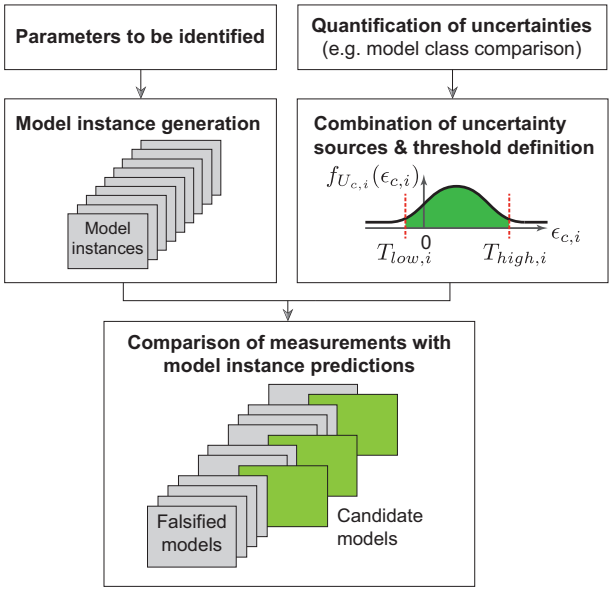

Figure 11. Flowchart summarizing the steps involved in the Grand-Mere Bridge diagnosis.

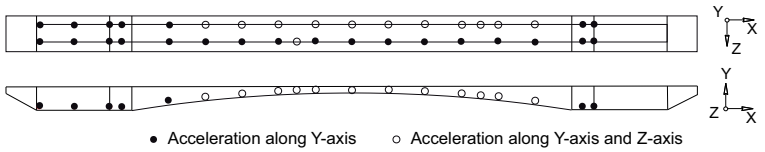

Figure 12. Accelerometer layout for Grand-Mere bridge monitoring system.

Michel et al. 2010). The six first singular values of the averaged power spectral density matrices (FDD spectrum) are shown in Figure 13. The number of singular values showing a peak in a given frequency range corresponds to the number of modes in this range. For instance, around the frequency 1 Hz, two singular values show a peak indicating the presence of two modes. The four first vertical modes represented in Figure 14 were identified with confidence. In addition, the first transverse as well as the first torsion modes are identified, but with a lower accuracy in the mode shape. The low number of components recorded in the transverse direction and the low amplitude of vibration in this direction led us to dismiss the transverse mode in the following analyses. In any case, not including a mode in the model-falsification process is conservative. Predicted and measured mode shapes are compared using the MAC test to verify that the comparison of natural frequencies is performed over the right modes.

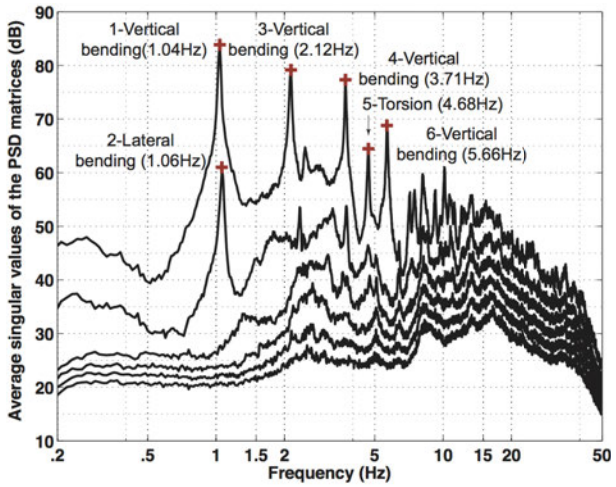

Figure 13. Averaged singular values of the power spectral density matrices for Grand-Mere Bridge.

Modes number 1, 3, 4 and 6 passed the MAC test with value larger than 0.8.

Parameter values to be identified and model instance generation

A sensitivity analysis revealed that predicted natural frequencies are most sensitive to variation in the concrete Young's modulus, in the bearing device condition, and in the level of cracking (see Figure 15 & Table 2). These structural properties are chosen as parameter values to be identified. For the Young's modulus, the value sought (E0) is an average over the structure. The bearing device condition is described by a parameter accounting for the possibility that longitudinal support displacement may be restrained under ambient vibrations due to friction forces as shown for another structure by Goulet et al. (2012). This phenomenon is simulated using longitudinal springs having unknown stiffness constants (K).

Finally, the possibility that cracked zones affect the behavior of the structure is tested by reducing the Young's modulus of concrete in regions located on the upper flange at the intermediate supports and on the lower flange at mid-span. This simplified representation of the cracking mechanism is intended to identify the eventual presence of undetected cracks. Five parameters are selected to describe these zones: an effective Young's modulus of the cracked concrete for each zone (E1, E2, E3) is expressed as a fraction of the average Young's modulus (E0); the length of the effective cracked zones at the supports (L1), and the length of the effective cracked zone at mid-span (L2). Overall, there are seven parameters that need to be identified as shown in Figure 15. The values used for each parameter are presented in Table 2.

An initial model set is made of 2187 (3^7) combinations of these parameters. These combinations were selected over a seven-dimensions grid where each parameter value

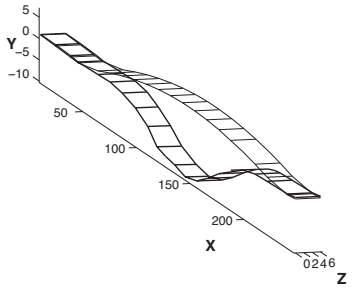

(a) Mode shape number one - Vertical bending (1.04Hz)

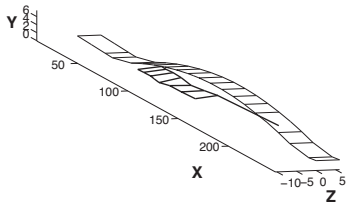

(b) Mode shape number two - Lateral bending (1.06Hz)

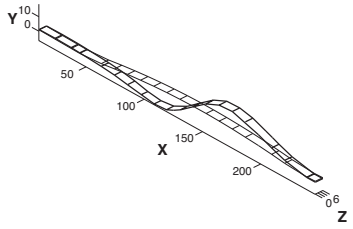

(c) Mode shape number three - Vertical bending (2.12Hz)

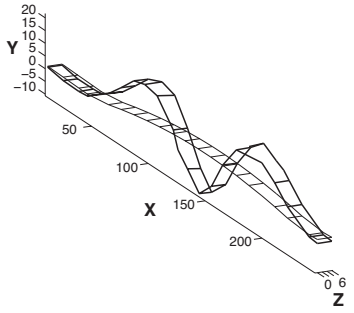

(d) Mode shape number four - Vertical bending (3.71Hz)

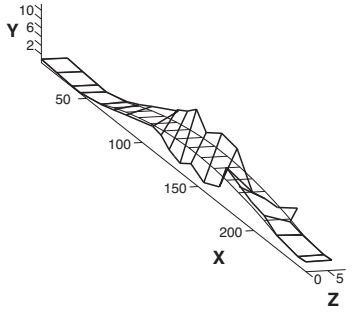

(e) Mode shape number five - Torsion (4.68Hz)

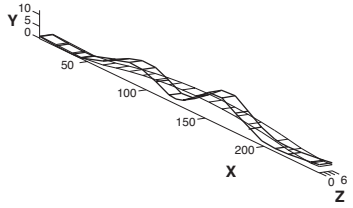

(f) Mode shape number six - Vertical bending (5.66Hz)

Figure 14. Measured mode shapes and frequencies for Grand-Mere Bridge. Each mode is shown with the undeformed profile.

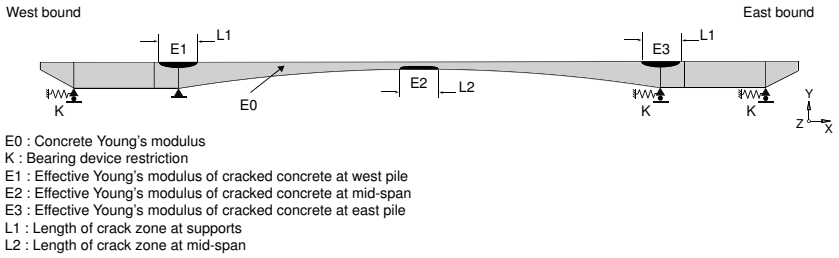

Figure 15. Parameter values to be identified for the Grand-Mere Bridge.

Table 2. Values for parameters (3 for each parameter) used to create the initial model set for the Grand-Mere Bridge.

Parameter value to be identified	Units	Values
Concrete Young's modulus (E0)	GPa	{15, 27.5, 40}
Bearing device restriction (K)	kN/mm	{0, 2E2 2E4}
Effective value of Young's modulus of cracked concrete at west pile (E1)	-	{0.1, 0.5, 1}
Effective value of Young's modulus of cracked concrete at mid-span (E2)	-	{0.1, 0.5, 1}
Effective value of Young's modulus of cracked concrete at east pile (E3)	-	{0.1, 0.5, 1}
Length of crack zone over supports (L1)	m	{4, 10, 16}
Length of crack zone at mid-span (L2)	m	{4, 10, 16}

can take the lower, higher and midrange of its interval. This choice of discretization is governed by the computing time. From the three model classes available, the shell-based class is chosen as a template model to evaluate the predictions for each instance of the initial model set. It has been shown in the previous section that except for torsional modes, the shell-based model adequately captured the dynamic characteristics of the solid-based model. It took 48 hours to evaluate the 2187 model instances using a workstation having 48GB of ram memory and two Intel Xenon X5560 8-core processors. Solving these models is computationally demanding. When computation time exceeds available resources, other stochastic sampling and surrogate modeling techniques could be used (Tarantola 2005; Sudret and Der Kiureghian 2000).

Uncertainties

Secondary parameters are those that have a marginal effect on the structural response and are considered as uncertainties. Natural frequencies are influenced by the mass and the rigidity of the structure. Therefore, the secondary-parameters are the concrete, pavement, and sand-filling densities, the pavement Young's modulus and the steel reinforcement Young's modulus. Except for the uncertainty attributed to the steel Young's modulus that follows a Gaussian *pdf* with a mean of 202 GPa and a standard deviation of 6 GPa, other secondary-parameter uncertainties are represented by uniform *pdf*s. Uniform *pdf* is used because, based on the principle of maximum entropy, it corresponds to the lowest level of information it is possible to represent in a proba-

bility distribution (Jaynes 2003). The details of each uniform uncertainty distribution are presented in Table 3. These uncertainties on secondary parameters are propagated in the template model to obtain the uncertainties associated with predicted frequencies. During this process, parameter values to be identified are set to their mean value.

Table 3. Secondary-parameter uncertainties for Grand-Mere Bridge.

Uncertainty source (Uniform distribution)	Unit	min	max
Concrete density	T/mm^3	2.2E-9	2.6E-9
Pavement Young's modulus	MPa	1000	10000
Pavement density	T/mm^3	2.0E-9	2.4E-9
Sand density	T/mm^3	1.1E-9	2.0E-9

Details of other uncertainty sources are summarized in Table 4. These sources are

Table 4. Other uncertainty sources for Grand-Mere Bridge.

Uncertainty source (Extended uniform distribution)	Lower bound	Upper bound	β
AVM epistemic variation	-2%	2%	0.30
Model simplifications			
Mode 1	-8%	-1%	0.30
Mode 3	-8%	-1%	0.30
Mode 4	-7%	-0%	0.30
Mode 6	-9%	-2%	0.30
Mesh refinement	0%	1%	0.30
Additional uncertainties	-1%	1%	0.30

described by the extended uniform distribution (Goulet et al. 2012). This distribution includes uncertainty regarding the bounds defining the uniform distributions. The parameter β represents the uncertainty of bound positions as a fraction of the initial interval width. The element discretization error is estimated based on a mesh refinement analysis conducted to determine the maximal plausible prediction error for each natural frequency. As for other quantities that were compared in the previous section, the mesh refinement error was found to be below the upper bound fixed at 1% of the predicted value. The evaluation of uncertainties related to model simplifications is based on the study presented in the previous section. Measurement variability is described by a Gaussian distribution with a mean of 0% and a standard deviation of 2%.

Model simplification errors are epistemic in nature because they are due to a lack of knowledge. A Bayesian interpretation of probability is used to define *pdf*s expressing the degree of belief of observing specific error values. An uncertainty of $\pm 4\%$ is added to the errors estimated in the previous study to represent that the solid-based model used as reference is also an approximation of the real structure.

Based on values reported in previous studies (Goulet et al. 2012), the ambient vibration monitoring epistemic variability is represented by an extended uniform distribution with bounds at $\pm 2\%$ of the measured frequency values. Observed variability across the datasets is represented by a Gaussian distribution having a standard deviation of 2% of the measured frequencies. This number is an upper bound based on previous experiments (Goulet et al. 2012).

All uncertainty sources are combined together using a Monte-Carlo process to obtain threshold bounds for each mode. Thresholds are computed for a target reliability $\phi = 0.95$. The relative importance of uncertainties is shown in Figure 16. The heights

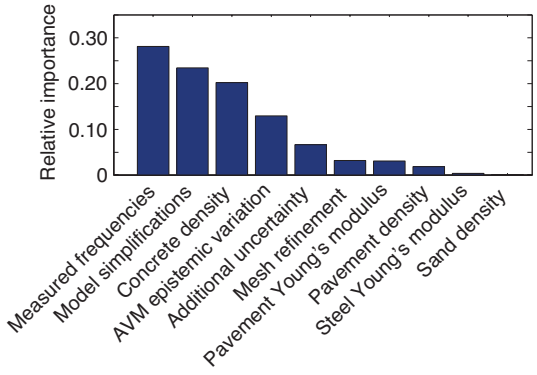

Figure 16. Uncertainty sources relative importance for Grand-Mere Bridge

of bars are the values of slope coefficient that are calculated from linear regression where observations are the combined uncertainty values obtained from a Monte-Carlo analysis using the normalized individual error values as input parameters. Error values are normalized such as the values corresponding to the lower endpoints having a probability content of 2.5% and the upper endpoints having a probability content of 97.5% correspond respectively to -1 and 1. The most important sources of uncertainty are measured frequencies, model simplifications and concrete density.

Model falsification

Figure 17 presents for modes 1, 3, 4 ,and 6 measured natural frequencies and predictions from all the model instances classified as either candidate or falsified models. Model instances are represented on the horizontal axis, and the predicted and measured values are shown on the vertical axis. The position of each dot corresponds to a prediction given by a model instance. The horizontal continuous line is the measured natural frequency, the two dashed lines are the threshold bounds that separate candidate and falsified model instances, and the vertical continuous line represents the magnitude of the probability density function of the combined uncertainty. Cross signs

represent candidate models, i.e. model instances whose predictions are simultaneously included between the threshold bounds for all modes $\{1, 3, 4, 6\}$. Some models that lie within threshold bounds for a given mode are falsified because they are outside the thresholds for other modes. Using multiple natural frequencies to compare predicted and measured values thus helps reduce the number of candidate models.

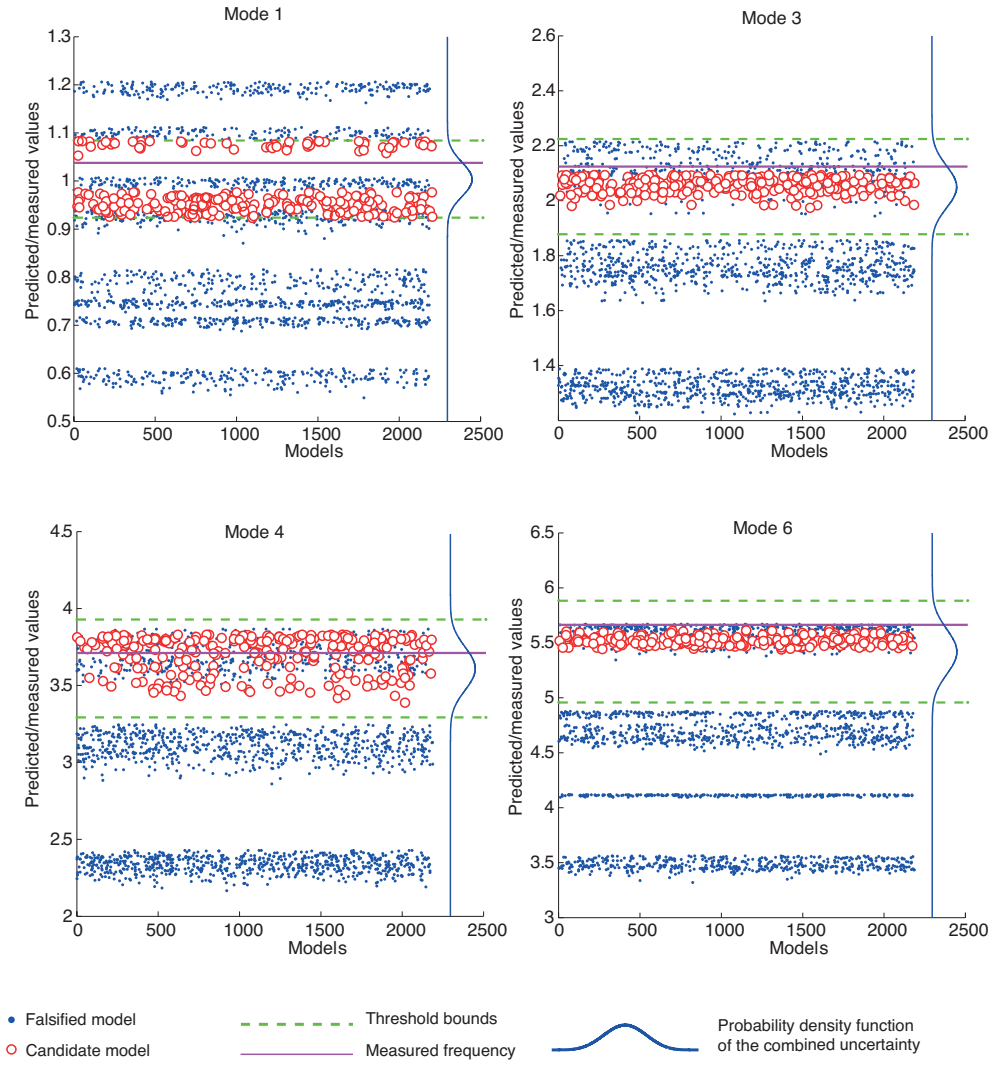

Figure 17. Comparison between the measured and predicted frequencies for modes 1, 3, 4 and 6 for the Grand-Mere Bridge.

The predicted frequencies for modes 3, 4 and 6 are influenced by the value of the concrete Young's modulus. The plots for modes 3, 4 and 6 in Figure 17 show distinct groups of predictions related to the three possible values for this physical parameter.

Model instances are falsified in a similar way for these three modes : models having the high value of 40 GPa for the concrete Young's modulus are selected as candidates for these modes. The first mode falsifies model instances in a different way. The scatter in model predictions for the first mode is influenced by a combination of the Young's modulus and the bearing device movement parameters. Models with a low and moderate value for concrete Young's modulus (15-27.5 GPa) are discarded regardless of the level of cracking and bearing device restriction.

A pairwise representation of the parameter values for the candidate model set is presented in Figure 18. Each graph represents the possible range for each parameter and dots correspond to candidate models. All 258 candidate models have a high value for concrete Young's modulus (E0). Some of these candidates models showed that the midrange value for the bearing device stiffness is possible when combined with a high level of cracking. All parameter values are possible for other parameters (E1, E2, E3, L1, L2). These plots show that even if the number of candidate models was reduced by more than 80% compared with the initial model set, the parameter range could only be reduced for the Young's modulus and for the beading device restriction.

The ranges of values identified for the concrete Young's modulus and the parameters related to the crack pattern can be used to obtain long-term creep and shrinkage behavior predictions with the template model. In accordance with results found in another study by Goulet et al. (2012), the identification shows that the bearing device behavior could have been hindered during ambient vibration monitoring. For ambient vibrations, restricting the longitudinal movement of bearing devices mainly affects the first vertical bending mode. Although the bearing device parameter can influence the structure under ambient vibrations, it is likely not to have an effect on its displacement under high loads and over a long time-span. Therefore, this parameter could be removed when performing long-term behavior simulations. The system identification study can support future long-term behavior simulations such as those performed by Bazant et al. (Bazant and Baweja 2000; Bazant et al. 2010; Bazant et al. 2008) on similar structures. Parameter values identified in this study are specific to the structure tested and results cannot be directly extrapolated to other structures. Nevertheless, the same methodology can be used.

DISCUSSION

Results obtained from the comparison of different levels of model complexity show that model simplifications systematically affect predictions at several locations and for several prediction types. When relationships between prediction errors lead to biased models, traditional system identification approaches that adjust parameter values in order to minimize the discrepancy between predicted and measured values may have difficulties to identify physically meaningful parameter values. Neglecting systematic errors, such as those described in this study, is likely to lead to wrong estimations for parameter values. Indeed, neglected model simplification errors and the effect of

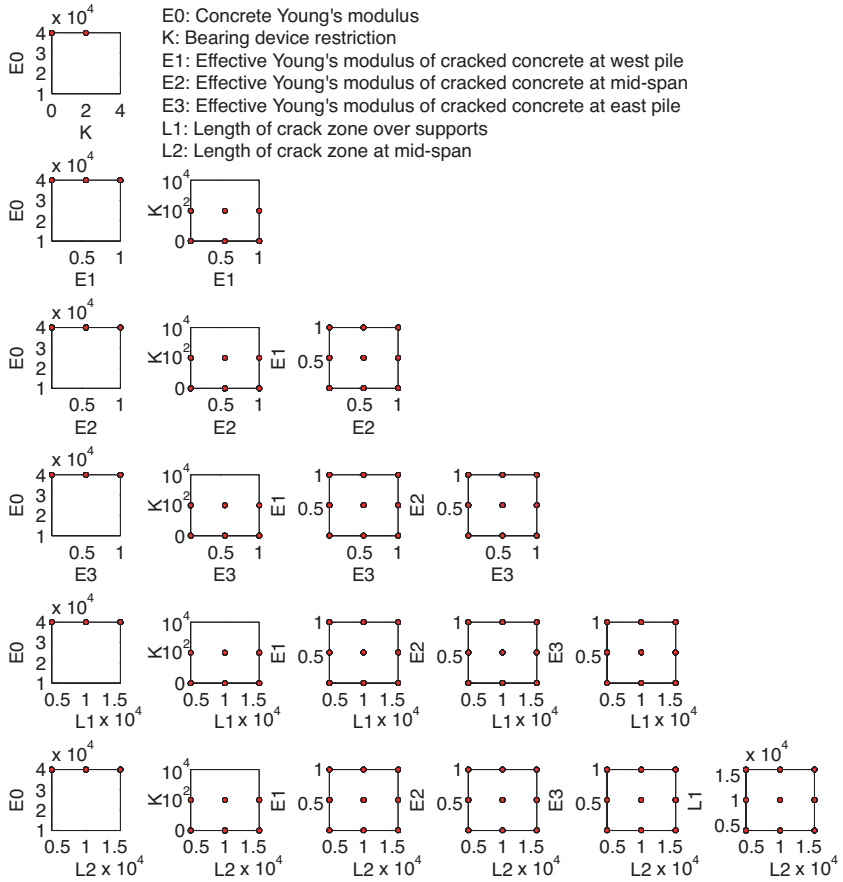

Figure 18. Pairwise representation of the candidate model set parameter values for Grand-Mere Bridge.

wrong parameter values may compensate for each other giving the illusion that the model predictions fit the measured data in an acceptable way.

Recognizing, quantifying and including uncertainties are important challenges of structural identification. Attempts to provide lower bounds for model simplification uncertainties are possible through the comparison of several orders of model complexity. Even if it is not specifically studied in this paper, it is acknowledged that there are tradeoffs between model complexity and identification accuracy. More complex models may reduce uncertainties leading to more precise diagnosis. However, this could involve higher computing and modeling costs. Further research is needed to quantify optimal tradeoffs.

CONCLUSIONS

The effect of modeling simplifications on prediction uncertainties is evaluated in order to improve structural identification. This study provides a starting point for a

model-based assessment of the Grand-Mere Bridge. Specific conclusions of this research are:

1. Model simplifications such as the degree of refinement of a model and the exclusion of secondary features have a significant influence on prediction errors. These errors are systematic and inter-dependent. Representing these by zero-mean independent Gaussian noise does not describe the relationships between errors observed in this case study.
2. Simplified models of the Grand-Mere Bridge inadequately represent local behavior. Errors in longitudinal strain predictions are in many cases significant ($>100\%$). Therefore, global behavior such as natural frequencies, displacements and rotations around the transversal axis are more appropriate quantities to be compared with measurements. Results from this study give lower bounds of model simplification error estimates that can then be used as input for system identification.
3. Two possibilities are identified for the behavior of structures based on ambient vibration monitoring data. Either the structure has a partial longitudinal hindrance in the bearing device combined with a high level of cracking or no longitudinal hindrance with several possible levels of cracking. All candidate models identified have a high value of Young's modulus.

ACKNOWLEDGEMENTS

The authors would like to thank Jean-Francois Laflamme and the Quebec transportation ministry (MTQ) for their contributions to the example of the Grand-Mere bridge. This research is funded by the Swiss National Science Foundation under contract no. 200020-117670/1.

References

Allemang, R. and Brown, D. (1982). "A correlation coefficient for modal vector analysis." *Proceedings of the 1st international modal analysis conference*, Vol. 1, Schenectady, NY, USA, Union Coll, 110–116.

Bazant, Z. and Baweja, S. (2000). "Creep and shrinkage prediction model for analysis and design of concrete structures: Model b3." *ACI Special publications*, 194, 1–84.

Bazant, Z., Li, G., Yu, Q., Klein, G., and Krıstek, V. (2008). "Explanation of excessive long-time deflections of collapsed record-span box girder bridge in Palau." *Proceedings of the 8th Int. Conf. on Creep, Shrinkage and Durability of Concrete and Concrete Structures, T. Tanabe et al., eds., The Maeda Engineering Foundation, Ise-Shima, Japan*, 1–31.

Bazant, Z., Yu, Q., Li, G.-H., Klein, G., and Kristek, V. (2010). "Excessive deflections of record-span prestressed box girder: Lessons learned from the collapse of the koror-babeldaob bridge in palau." *ACI Concrete International*, 32(6), 44–52.

Brincker, R., Zhang, L., and Andersen, P. (2001). "Modal identification of output-only systems using frequency domain decomposition." *Smart Materials and Structures*, 10, 441–445.

Catbas, F., Kijewski-Correa, T., and Aktan, A. (2012). *Structural Identification of Constructed Facilities. Approaches, Methods and Technologies for Effective Practice of St-Id*. American Society of Civil Engineers (ASCE).

Eamon, C. and Nowak, A. (2004). "Effect of secondary elements on bridge structural system reliability considering moment capacity." *Structural Safety*, 26(1), 29–47.

Goulet, J., Michel, C., and Smith, I. (In press, 2012). "Hybrid probabilities and error-domain structural identification using ambient vibration monitoring." *Mechanical Systems and Signal Processing*.

Jaynes, E. (2003). *Probability theory: The logic of science*. Cambridge Univ Press, Cambridge, England.

Massicotte, B. and Picard, A. (1994). "Monitoring of a prestressed segmental box girder bridge during strengthening." *PCI Journal*, 39(3), 66–80.

Massicotte, B., Picard, A., Gaumond, Y., and Ouellet, C. (1994). "Strengthening of a long span prestressed segmental box girder bridge." *PCI Journal*, 39(3), 52–65.

Michel, C., Guéguen, P., and Bard, P.-Y. (2008). "Dynamic parameters of structures extracted from ambient vibration measurements: An aid for the seismic vulnerability assessment of existing buildings in moderate seismic hazard regions." *Soil Dynamics and Earthquake Engineering*, 28(8), 593–604.

Michel, C., Guéguen, P., El Arem, S., Mazars, J., and Kotronis, P. (2010). "Full-scale dynamic response of an rc building under weak seismic motions using earthquake recordings, ambient vibrations and modelling." *Earthquake Engineering & Structural Dynamics*, 39(4), 419–441.

Mottershead, J., Link, M., and Friswell, M. (2011). "The sensitivity method in finite element model updating: A tutorial." *Mechanical Systems and Signal Processing*, 25(7), 2275–2296.

Nowak, A. and Carr, R. (1985). "Sensitivity analysis for structural errors." *Journal of Structural Engineering*, 111(8), 1734–1746.

Nowak, A. and Szerszen, M. (1998). "Bridge load and resistance models." *Engineering structures*, 20(11), 985–990.

Oberkampf, W. and Trucano, T. (2008). "Verification and validation benchmarks." *Nuclear Engineering and Design*, 238(3), 716–743.

Sankararaman, S. and Mahadevan, S. (2011). "Model validation under epistemic uncertainty." *Reliability Engineering & System Safety*, 96(9), 1232–1241.

Šidák, Z. (1967). "Rectangular confidence regions for the means of multivariate normal distributions." *Journal of the American Statistical Association*, 62, 626–633.

Sudret, B. and Der Kiureghian, A. (2000). "Stochastic finite element methods and reliability: a state-of-the-art report." *Report No. UCB/SEMM-2000/08*, University of California Berkeley, Dept. of Civil and Environmental Engineering, Berkeley,

CA.

Tarantola, A. (2005). *Inverse problem theory: Methods for data fitting and model parameter estimation*. Siam, Philadelphia, PA, USA.

Topkaya, C., Kalayci, A., and Williamson, E. (2008). "Solver and shell element performances for curved bridge analysis." *Journal of Bridge Engineering*, 13(4), 418–424.